Tuijin Jishu/Journal of Propulsion Technology
ISSN: 1001-4055
Vol.47 No.01(2026)

# Heuristic Approach for Distortion Free Weld Defect Detection

**[1] K Gopi Chand, [2] G V RAMBABU**

[1]M.Tech , Thermal Engineering ,

MLR Institute of Technology,

Dundigal, Hyderabad

[2]Associate Professor, Dept of Mechanical,

MLR Institute of Technology,

Dundigal, Hyderabad

**Abstract:** Numerous fields make extensive use of non-destructive testing (NDT). In NDT, weld line defect detection is highly common. Most weld lines, particularly those found in pipes, ships, airplanes, etc., should be inspected before being used. The X-ray method is one of the mainly used approaches in the field of welding flaw inspection. These tasks can now be delegated to a computer thanks to advancements in computer technology and image processing techniques. The weld line is not flat, though. As a result, there is variation in the image backgrounds. Additionally, the flaws are always quite minor. Radiography picture interpretation is challenging because of the small size of the faults and the deteriorated quality. This work presents an automatic approach for identifying welding flaws in radiography pictures. To enhance the quality of the radiography image, image preprocessing is used after the digital radiographs are obtained. A fuzzy entropy oriented multi-level thresholding technique is suggested. This approach uses highest fuzzy redundancy to process the radiography image in order to enhance both the detection accuracy and imaging quality.

**Keyword-** Weld defect detection, learning approach, distortion free and system accuracy.

## I. INTRODUCTION

The majority of structural failures, including ship sinking, building failure, base settlement, and airplane accidents, are precede by a number of caution, frequently too faint to be heard or seen without assistance. We can read these warnings thanks to non-destructive testing (NDT) [1]. From quality control of new construction to as-built condition verification forecast and demolition monitoring. NDT technologies are helpful at every stage of a structure's life. All fields use non-destructive testing (NDT) techniques, which measure specific physical characteristics of equipment or construction and then infer or deduce related attributes to get the necessary information. Data reduction and analysis are essential to each approach. The bounds of NDT are unclear. Non-destructive testing includes basic methods like visual inspection and possibly the measurement of a physical attribute that is difficult to identify. Radiography, ultrasonic, magnetic, electrical, and penetration were once thought to be the five main techniques, however each of these can be further subdivided [2]. Many NDT techniques have advanced to the point where a competent operator may utilize them by following thorough procedural instructions. NDT is necessary to offer precise defect size information as well as highly reliable defect detection. It can be used to a broad variety of materials and constructions, including welding. Welded structures frequently require non-destructive testing because weld metal flaws compromise the strength of the welded connection. This is especially true for essential applications where a weld failure might be disastrous, like pressure tanks, load-bearing structures, power plants, and pipelines. Welded constructions must be inspected to make sure the weld quality satisfies design and operation specifications, guaranteeing dependability and safety. Welding faults can be inspected using a range of NDT techniques [3]. It is predicated on X-rays' capacity to penetrate

materials that are opaque to normal light, such as metal, and use the radiant energy they transfer to create photographic records [4]. It should come as no surprise that radiography has developed into a sophisticated technology over the course of the approximately 100 years that the fundamental physical principles of radiographic inspection have been understood [5]. If the interpreter is knowledgeable with the manufacturing process and component or part configuration, he will be able to make wise decisions [6]. [7]. [8] offered a multi-step technique for separating radiography background pictures with fault indications. The technique was created to preserve the specifics of the defects while eliminating the general backdrop structure. [9] suggested a curve fitting-based method for detecting welding flaws. [10] suggested a multi-layer perceptron neural network with fuzzy k-nearest neighbour to categorize various kinds of welding flaws. Five components made up the entire system: pattern classification, feature extraction, defect segmentation, contrast enhancement, and noise reduction. The radiography image noise was reduced using the median filter [11]. To improve the contrast, the histogram equalization procedure was used. Using the background subtraction approach and the histogram thresholding method, defect segmentation was used to remove flaws from the background. A fuzzy skilled scheme for the categorization of welding breaks was subsequently created by [12]. For every entity in the line picture, three features were derived: width, mean square error and highest intensity. [13] Suggested an automated welding flaw identification approach. The X-ray image quality was initially improved by applying the median filter and contrast enhancement approach. The X-ray image was then segmented to identify any possible flaws. The following geometric and gray value properties were extracted: roundness, aspect ratio, width area ratio, length area ratio, contrast, and location. A linear discriminate classifier was trained using the most pertinent features as input data. [14] Introduced a k-nearest neighbour classifier-based automated welding flaw detection technique. A pattern recognition algorithm was used for the detection:

i) Segmentation: a watershed method and morphological procedures [15] were used to identify pixel regions and segregate them from the remainder of the X-ray image.

ii) Feature extraction: form properties (width dissimilarity and principal direction of inertia refereeing to invariant moments) were summarized and the regions were measured. iii) Classification: a k-nearest neighbour classifier was used to examine and categorize the retrieved attributes of each region [16]. The authors claim that the method's detection rate was good. [17] Suggested automatic flaw identification with statistical classifiers and textural characteristics. The three stages of the suggested approach were feature extraction, categorization, and segmentation of possible defects. Segmentation was the initial step. It made use of the laplacian of Gaussian (LoG) [18,19] edge detector. At the moment, every radiograph must be manually read by a qualified translator and preserved as a film. Film radiography-based human interpretation of weld quality is highly arbitrary, erratic, time-consuming, and occasionally biased. Additionally, it could be required to recheck the film after a while. Finding a movie among the many that are kept gets much more difficult as a result. The films' quality will eventually decline as well. Under dynamic distortion conditions, this results in complex filtration and misclassification.

## II. WELD DEFECTION DETECTION

Although the industry provides most of the specifications for defect type, minimum defect size, and acceptance criteria, the knowledge regarding acceptability is ambiguous because no actual control is done on the weld. No matter how big or small, cracks are undesirable, thus that's the only information that can be considered absolute. A weld line can have a variety of flaws.

1. **Porosity:** This is the result of gas trapped in the weld metal creating voids. The voids can appear in random, clustered, or linear patterns and as spherical, elongated, or "wormhole" shapes. Spherical voids appear as a rounded black region on the radiograph, but non-spherical cavities have an stretched out shady region with a even boundary.
2. **Slag Inclusions:** These are slag particles trapped along the fusion planes or in the weld metal. The particles may be irregularly shaped or extended in the direction of the settled weld droplet, and they seem darker than the surrounding area.
3. **Lack of Fusion:** This discontinuity occurs when molten weld metal fails to fuse to a formerly settled weld droplet or to the base metal. It shows up on the radiograph as a dark signal that is often elongated and varies in breadth.

4. **Cracks:** A solidified metal rupture. Welding cracks can be longitudinal, transverse, or radically oriented, and they can happen in the base metal, the weld metal, or both. It appears as continuous, irregular, or sporadic lines on the radiograph.
5. **Incomplete Penetration:** When complete penetration has not been attained, a discontinuity at the root of welds intended for thorough penetration occurs. On a radiograph, the discontinuity shows up as a straight, black line that could be intermittent or continuous.
6. **Burn through**: This occurs when the metal melts through the backing strip or from the weld's root. On the radiograph, it shows up as a single, black patch of rounded or elongated shape that could have a lighter ring around it.

Figure 1: Radiographic image instance in a weld P-Ray

The gray level difference alone cannot identify the flaws. An optimal outcome cannot be achieved with a single approach.

A CNN-based technique using ResNet50 as the foundation model was introduced in [20] for building a deep learning approach in weld fault identification. This method substituted four additional completely connected layers for the final classification level. The yield of the last convolutional level of the previously inserted ResNet50 network is fed into the first layer, a 2D Global Average Pooling layer. Then, to lower dimensionality and extract more intricate and abstract information from the pictures, a dense layer of 512 neurons with ReLU activation function is employed. A 50% dropout level was put after the thick level to prevent overfitting. During training, dropout "deactivates" neurons at random, which helps to regularize the model and lessen reliance on particular features. Four neurons were added to the final dense layer, representing the four classes of weld flaws that needed to be categorized. A softmax activation function is used in this layer to assign probabilities to each class and enable classification. Using transfer learning for feature extraction and fine-tuning for task-specific adaptation, a model with enhanced capacity for classifying weld flaws in radiographic images was thus produced. However, a significant number of weld defect detections are misclassified due to the dynamic and semantic character of the distortion.

## III. ADAPTIVE DENOISING AND DEFECT DETECTION USING DEEP FUZZY INTERFACE

Using the previous framework as a guide, a robust intelligent system for identifying defects in welding is constructed. Creating a novel algorithmic strategy for the preprocessing, segmentation, representation, and classification processes is the main goal of this work. The system architecture is created for the purpose of detecting and classifying welding. Figure 2 illustrates the system architecture that has been designed for intelligently detecting defects in welding.

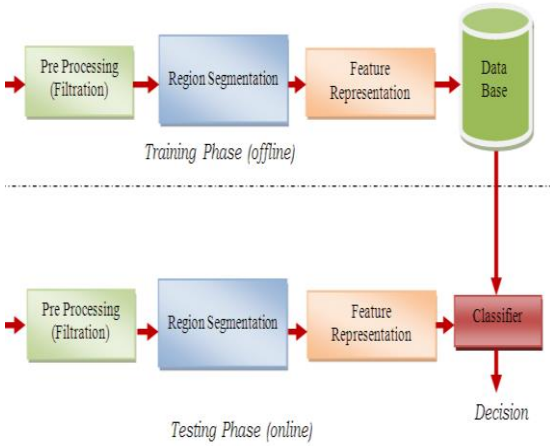

Figure 2. System Architecture for DefectWeld identification using intelligent system

In order to remove distortion effects at the pre-processing stage, the denoising procedure has been seen in a variety of genres. Among the various feature extraction techniques, GLCM features were most frequently employed in more recent methodologies.
This method's threshold computation is dynamic, utilizing fuzzy-based assessment for varying noise difference for the detection process. However, the method that is being provided does not offer any criteria for dynamic noise levels or for preventing artifacts in the median filter. The processing levels govern the preservation of finer details because accuracy preservation is fundamental. The median filter strategy ignores the noise distribution characteristic in noise reduction and is limited to defined blocks, which adds complexity in computation. The classifier model makes use of a system-following learning mechanism. The current system explains the centroid for the classifier model using a clustering method. On the other hand, as the amount of learning information increases, the strategy becomes more constrained. For example, k-mean template look for has a thorough examination under semantic area.
Two-phase algorithms are presented by such an algorithm. This algorithm separates the damaged and undamaged pixels using a median filter construction. In the second step, noise processing is also recommended, and noise quality regulation is distinct. The primary disadvantage of this approach is that it requires a huge window size in two steps to provide the right output, which results in a very high processing time. There will also be circuits that are more complicated. Better details are not acceptable distortions, and this technique is not well adapted for high densities. Based on how the restrictions are fixed, an adaptive distortion filter is recommended. In order to examine the estimations for the distortion impact computation, assumptions about a system are developed. In the Gaussian distortion, the spectral density is precisely determined. In order to reduce Gaussian noises in image processing, denoising filters were created.

**a) FILTRATION PROCESS**

To identify the mass area, a variety of image processing filter variations are applied to the detection image. The median filtering technique is particularly effective in suppressing brief noise. As may be observed, median filters prevent noise from obscuring edges by introducing imbalanced operators for noise removal. However, the image's borders and many finer details are likewise blurred by numerous weld image processing filters. It is typically seen when data is received from communication channels or camera sensors. To remove noise, a mean filter's basic filtration is employed. The function is used by the mean filter given as,

$$F_{mn} = \frac{1}{r \times c}\left(\sum_{i=1}^{r}\sum_{j=1}^{c} p_{i,j}\right) \quad (1)$$

Where the noise of an observing area is suppressed using the mean variable of the observing region. The magnitude monitoring limits its usage and median filters are used. The median filter is defined as,

$$F_{md} = avg(|p_{i,j}|^2) \quad (2)$$

The outline of revision among a position and the rest of positions in a median filter is given as,

$$P_{df}(P,p) = \left(1 - \frac{1}{V-1}\left|\sum_{i=1}^{V}\frac{P-p_i}{|P-p_i|}\right|\right) \quad (3)$$

These filtration methods offer poor processing performance due to several types of noise distortion. A consistent method called Time-Domain Median Filter seeks to eliminate distortion from weld images while keeping the edges that exhibit significant distortion.
However, these filters' fixed block restricts how they can be used for different image processes. Image data is eliminated in places without references, which affects the image content. After a specified amount of time, each decision point is computed. The MSE-Optimized Stationary linear filter is used to determine the Adaptive Spectral Median Filter. To remove noise, a dynamic spectral filter is used in the occurrence area. However, the procedure can only be used under non-variant conditions, which restricts its application to dynamic conditions. This paper develops a fuzzy-based decision-making method for denoising that takes into account the distribution of image pixels. In order to take out the distortion level in relation to variations in pixel intensity throughout a

distributed image region, this denoising technique is based on pixel density.

**b) DE-NOISE APPROACH**

Fuzzy logic has been shown to be a natural fit for weld defect monitoring. It leans to generalize existing classification techniques and their applications. The fundamental idea behind fuzzy logic is that real-world situations are not always accurate, so fuzzy used to do approximately a sample with cognitive abilities. An additional characteristic of fuzzy-based methods is that they do not correlate correlations between exact numerical quantities. Therefore, it is reasonable to argue that intelligent monitoring systems based on fuzzy logic (FL) should be chosen for the majority of weld defect applications.

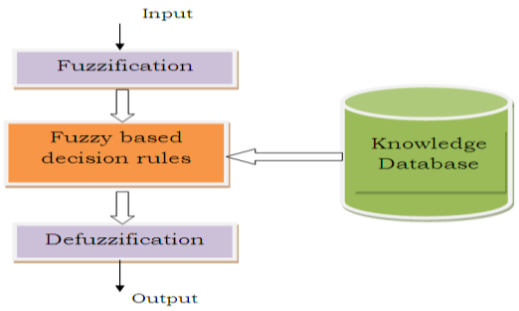


Figure. 3. Mechanism of fuzzy implication scheme

The likelihood allocation algorithm for image improvement make use of a fuzzy logic method by means of 5 constraint, that is α, $\beta_1$, γ, $\beta_2$ and be very successful as given away in Figure 4.

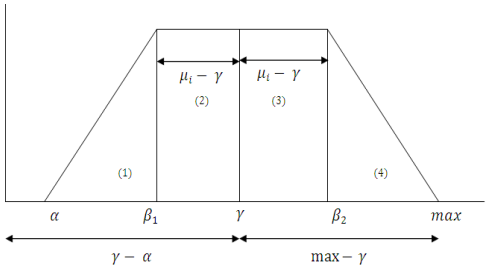


Figure 4. Likelihood allocation utility

The minimal value of the distribution is represented by "α," the average value by "γ," and the maximum value by "max," depending on the parameters required. The following is the definition of reducing β1 and β2 to improve image quality using the possibilities distribution algorithm. Giving the mean value γ, is how to accomplish this. Image denoising is done using fuzzy rules for the following enhancements:

1. $Condition - 1: If\ \xi \leq p(P,y) \leq \mu 1\ then,\ p(P,y) = 2\ ((p(P,y) - \xi)\ /\ (\alpha - \xi))2$
2. $Condition - 2: If \mu 1 \leq p(P,y) \leq \alpha\ then,\quad p(P,y) = 1 - 2\ ((p(P,y) - \alpha)\ /\ (\alpha - \xi))2$
3. $Condition - 3: If\ \alpha \leq p(P,y) \leq \mu 2\ then,\quad p(P,y) = 1 - 2\ ((p(P,y) - \alpha)\ /\ (highest - \alpha))2$
4. $Condition - 4: If \mu 2\ p(P,y) \leq highest\ then, p(P,y) = 2\ ((p(P,y) - \alpha)\ /\ (highest - \alpha))2$

Where $p(P,y)$ is the strength of the sample coefficient.

System that decreases the strength of coefficient that have values among $\mu_1$ and $\mu_2$ are symbolized by conditions 2 and 3. The procedure of the likelihood allocation algorithm is given as:

**Procedure -1: coefficient allocation**

- From the conditions, the least, highest and average values are leasted.

• Value of $\mu_1$ is allocated with the outcome of $(least + average)/2$

• value of $\mu_2$ is allocated with the outcome of $(average + highest)/2$

**Procedure -2: Fuzzification**

1. For every coefficient, apply conditions (conditions -1, conditions -2, conditions -3 and conditions -4) to obtain a fresh coefficient value

compute the average value of coefficient strength:

$$Avg = Avg2(coefficient) \quad (4)$$

**Procedure 3: Result process**

* resolve μ1 acquired from computation, (least + Avg) / 2 and μ2 acquire from computation (highest + avg) / 2 where,

Least: the least coefficient strength value in the sample

Highest: the maximum coefficient strength value in the sample

Avg: the average value of coefficient strength in the sample

$$C1 = (least + Avg)/2; \quad (5)$$

$$C2 = (Highest + Avg)/2; \quad (6)$$

For all coefficients in the coefficient matrix, Fuzzification is performed out using defined conditions:

**1.** If the coefficient is superior than the value of least and coefficients are low than the value of μ1, then the coefficient level is modified to 2 ((coefficient -least) / (avg-least)) 2

$if\ (coefficient\ (i,j) = least)\ \&\&\ (coefficient\ (i,j) < C1)$

$new\ coefficient\ level(i,j) = 2 * (((coefficient\ (i,j) - least)/(Avg - least))\text{^}2);$

**2**. If the coefficient is larger than the value of μ1 and coefficients are low than the avg. value, the coefficient level is modified to $1 - 2\ ((pixel - least)\ /\ (Avg - least))\ 2$

$if\ (coefficient\ (i,j) >= C1)\ \&\&\ (coefficient\ (i,j) < Avg)$

$modified\ coefficient(i,j) = 1 - (2 * (((coefficient\ (i,j) - Avg)/(Avg - least))\text{^}2));$

**3**. If the coefficient is bigger than avg and coefficients are lower than the value of μ2, then the coefficient level is modified to 1-2 ((coefficient -avg) / (highest-avg)) 2

$if\ (coefficient\ (i,j) >= Avg)\ \&\&\ (coefficient\ (i,j) < C2)$

$modified\ coefficient(i,j) = 1 - (2 * (((coefficient\ (i,j) - Avg)/(maks - Avg))\text{^}2))$

**4**. If the coefficient is larger than the value of μ2 and the coefficient is lower than highest, then the coefficient level is modified to 2 ((coefficient-avg) / (highest-avg)) 2

$if\ (coefficient\ (i,j) >= C2)\ \&\&\ (coefficient\ (i,j) < max)$

$modified\ coefficient(i,j) = 2 * (((coefficient\ (i,j) - Avg)/(maks - Avg))\text{^}2)$

**Procedure 4: change**

Compute each fuzzy coefficient for each value (coefficient level) powered by two.

$$fuzzycoefficient\ (i,j) = modified\ coefficient(i,j)\text{^}2 \quad (7)$$

**Procedure 5: Defuzzification**

For the entire coefficients in the sample, the coefficient that is modified is computed by multiplying coefficient with the strength of coefficient of each coefficient . The filtration is performed as:

1. If the centered value is included in the codebook vector $cv_j^*$, the coefficient is assigned to j*th cluster.

$$Cl_j(p_i) = 1\ if dis(p_i, c_j) = distance(p_i, c_j^*) \quad (8)$$

$$Cl_j(p_i) = 0\ if dis(p_i, c_j) \neq distance(p_i, c_j^*) \quad (9)$$

2. If the number of elements in the set $P_i^{(t)}$is more than one, then the membership function depends on the distance between xi and $c^j \in P_i^{(t)}$, that is$Cl_j(p_i) = f(distance(p_i, c_j), c^j \in P_i^{(t)})$have to suit subsequent conditions,

a) $Cl_j(p_i)$is a diminishing task of $distance(p_i, c_j)$

b) $Cl_j(p_i)$tends to one as $distance(p_i, c_j)$ tends to 0.

c) $Cl_j(p_i)$ tends 0 as $distance(p_i, c_j)$ tends to $dishighest(p_i)$

Where,

$$dishighest(p_i) = \underset{c^j \in P_i^{(t)}}{\text{highest}}\, distance(p_i, c_j) \quad (10)$$

Using a fuzzy operator is the same as fuzzifying inputs. The Sugeno Output membership functions, on the other hand, are linear or fixed. The Sugeno Fuzzy process is applied to vibrant block coding in this work. In conventional filtration, a elevated rank indicator is used in spite of center point to classify vectors according to a set of criteria. Whether or whether it is the main focus of the original data is not taken into account. The tragic event involving these filters is clever, and the image reflects this as well. Actual weld imaging data is needlessly eliminated in regions where no weld is absent.

$$V_c = (\text{P-}p_c\ ,\ \text{y-}y_c) \quad (11)$$

Where,

$$p_c = \frac{1}{N}\sum_{i=0}^{N-1}(p_i) \quad (12)$$

is middle position of P

and

$$y_c = \frac{1}{N}\sum_{i=0}^{N-1}(y_i) \quad (13)$$

Is the middle position of of y

Here, N is the whole amount of pixels.

## IV. SIMULATION RESULT

The analysis of the outlined method examination is made using PeakSNR, β, £ and Φ metrics. Here, $PeakSNR$ describe a ratio of actual coefficient strength over misrepresentation strength. The factor is presented by,

$$PeakSNR(dB) = 10log_{10}\left(\frac{P_{max}^2}{\beta}\right) \quad (14)$$

Where $P_{max}$ is the peak value of actual sample.

and β is the Mean square Error.

The Mean square error (β) is presented as the squared error of the filtered outcome to the actual examination sample. The PeakSNR presented the coefficient inference value, and β represents the mean deviation in the outcome as match up to the actual sample. The computation of β is given as ,

$$\beta = \frac{1}{x \times y} \sum (P - \hat{P})^2 \quad (15)$$

Here, $P$ is the actual processing sample, and $\hat{P}$ is the filtered output.,

The Root mean square error (£) factor is presented by the square root process of β value given by,

$$RMSE = \sqrt{\beta} \quad (16)$$

factor relative reconstruction error (Φ) is presented as the matching error of filter output to actual sample correlated over the actual sample given by,

$$\Phi = \sqrt{\frac{(P - \hat{P})}{P}} \quad (17)$$

The relative investigation of the outlined method and the observed factors are illustrated in Table 1 below.

Table 1: β Observations for different noise variances (ρ)

| Sample | Median coding | | | CNN-Coding [1] | | | CNN-Fuzzy coding | | |
|---|---|---|---|---|---|---|---|---|---|
| | 0.2 | 0.5 | 0.7 | | 0.2 | 0.5 | 0.7 | | 0.2 |
| P1 | 31.5 | 30 | 29.3 | P1 | 31.5 | 30 | 29.3 | P1 | 31.5 |
| P2 | 31.7 | 31.1 | 29.5 | P2 | 31.7 | 31.1 | 29.5 | P2 | 31.7 |
| P3 | 35.2 | 35.3 | 33.4 | P3 | 35.2 | 35.3 | 33.4 | P3 | 35.2 |
| P4 | 35.1 | 34.4 | 33.5 | P4 | 35.1 | 34.4 | 33.5 | P4 | 35.1 |
| P5 | 31.3 | 31.3 | 30.8 | P5 | 31.3 | 31.3 | 30.8 | P5 | 31.3 |

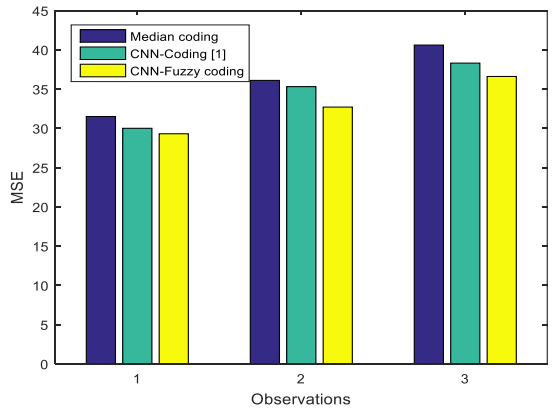


Figure 5. Developed approaches β observation

Table 2: varying noise variances PeakSNR Observations

| Sample | Median Coding | | | CNN-Coding [1] | | | CNN-Fuzzy coding | | |
|---|---|---|---|---|---|---|---|---|---|
| | 0.2 | 0.5 | 0.7 | 0.2 | 0.5 | 0.7 | 0.2 | 0.5 | 0.7 |
| P1 | 84.3 | 82.1 | 80.5 | 95.6 | 85.1 | 83.2 | 98.8 | 94.9 | 93.8 |
| P2 | 85.4 | 82.4 | 76.4 | 97.2 | 87.3 | 83.6 | 98.4 | 95.2 | 91.4 |
| P3 | 83.9 | 81.6 | 75.6 | 96.1 | 86.4 | 84.5 | 99.3 | 93.8 | 90.3 |
| P4 | 83.5 | 81.7 | 75.7 | 95.9 | 86.9 | 81.1 | 99.7 | 92.2 | 91.7 |
| P5 | 85.4 | 83.1 | 76.4 | 98.3 | 89.7 | 86.4 | 98.2 | 93.4 | 92.2 |

| Observing Sample | Median Coding | | | CNN-Coding [1] | | | CNN-Fuzzy coding | | |
|---|---|---|---|---|---|---|---|---|---|
| | 0.2 | 0.5 | 0.7 | 0.2 | 0.5 | 0.7 | 0.2 | 0.5 | 0.7 |
| P1 | 0.07 | 0.07 | 0.08 | 0.040 | 0.05 | 0.06 | 0.031 | 0.034 | 0.035 |
| P2 | 0.06 | 0.071 | 0.08 | 0.036 | 0.05 | 0.06 | 0.025 | 0.029 | 0.032 |
| P3 | 0.2 | 0.23 | 0.22 | 0.09 | 0.1 | 0.13 | 0.07 | 0.074 | 0.077 |
| P4 | 0.1 | 0.13 | 0.12 | 0.026 | 0.04 | 0.04 | 0.016 | 0.02 | 0.022 |
| P5 | 0.11 | 0.12 | 0.13 | 0.037 | 0.05 | 0.06 | 0.025 | 0.029 | 0.038 |

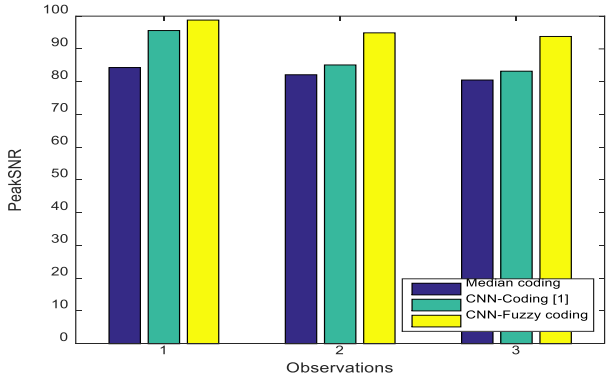


Figure 6. Developed approaches PeakSNR observation

Table3: Φ observations for varying noise variances

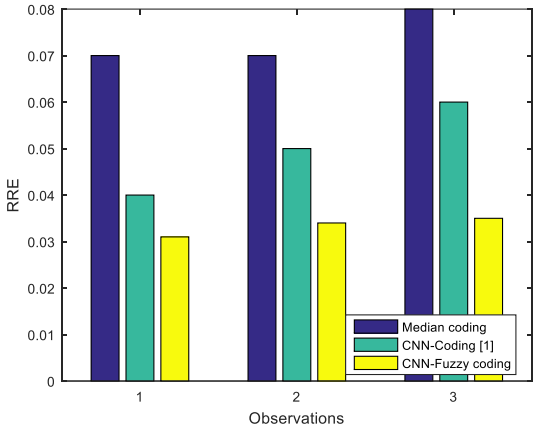


Figure 7. Developed approaches Φ observation

Observation for the developed approach for varying noise variance for the tested sample is illustrated below.

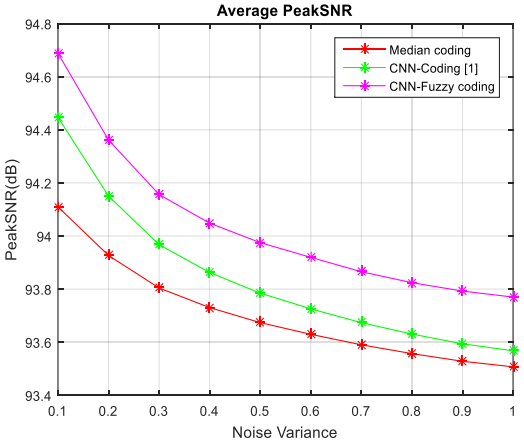


Figure 8. PeakSNR result observation

The outcomes demonstrate an enhancement in PeakSNR value by 25dB as measure up to the existing denoising approach. The PeakSNR is observed to be 18dB higher at a noise variance of 0.6. The relative measure of the £ value for the outlined method is shown in Figure 9.

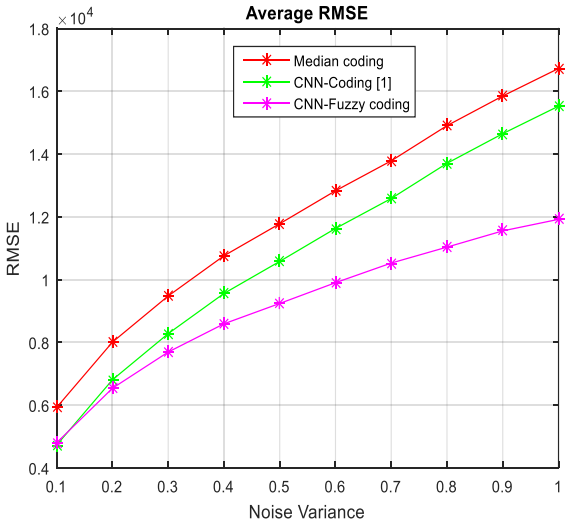


Figure 9. £ Result observation

At noise discrepancy σ = 0.6, the dynamic decision filter approach's £, which is calculated as the squared root of the β parameter, is found to be 3.51% lesser than the CNN filter's and 2.72% lower than the CNN filters. The program accurately detects each pixel and receives the appropriate data for that location in the sample when the £ value is zero. Figure 10 shows the relative reconstruction error (Φ) observation with changing noise variance.

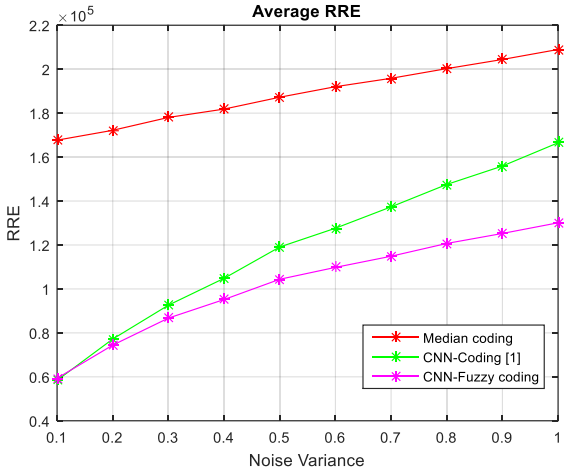


Figure 10. Φ result observation

Because the suggested method uses a dynamic choice for the noise filtration, it is found to have a smaller relative reconstruction error. Because fuzzy rules were used to produce the measurement noise level, the approach exhibits a decreased relative reconstruction error. Additionally, the estimation noise is resilient to large noise densities. This illustrates how accurate the suggested method's estimation.

## V. CONCLUSION

A fuzzy-based estimation-based denoising technique is suggested. For image coding employing the fuzzy set scheme, this method provides a choice using dynamic conditions, the filtration of noise by varying conditions is found to be additional resilient. Based on choices, this method provides a vibrant collection across a variety of discrepancy in the noisy situation. The suggested method shows a lower MSE factor and a greater PSNR when compared to the current mean, median filtration method. The acquired observations demonstrate how accurate the suggested approach's estimation is.

## VI. REFERENCES

[1] Palma-Ramírez, Dayana, Bárbara D. Ross-Veitía, Pablo Font-Ariosa, Alejandro Espinel-Hernández, Angel Sanchez-Roca, Hipólito Carvajal-Fals, José R. Nuñez-Alvarez, and Hernan Hernández-Herrera. "Deep convolutional neural network for weld defect classification in radiographic images." Heliyon 10, no. 9 (2024).

[2] K. Pal, B.V. Patel, Data classification with K-fold cross validation and Holdout accuracy estimation methods with 5 different machine learning techniques, in: 2020 Fourth International Conference on Computing Methodologies and Communication (ICCMC), 2020, pp. 83–87.

[3] S. Szeghalmy, A. Fazekas, A comparative study of the use of stratified cross-validation and distribution-balanced stratified cross-validation in imbalanced learning, Sensors 23 (4) (2023) 2333.

[4] M. Sofia and D. Redouane, “Shapes recognition system applied to the non destructive testing,” in Proceedings of the 8th European Conference on Non-Destructive Testing, Barcelona, June 2002.

[5] D. Mery and M. A. Berti, “Automatic detection of welding defects using texture features,” Insight, vol. 45, pp. 676–681, 2003.

[6] R. M. Haralick, K. Shanmugam, and I. Dinstein, “Textural features for image classification,”IEEE Trans. on Systems, Man, and Cybernetics, vol. 3, pp. 610–621, Nov. 2001.

[7] M. Amadasum and R. King, “Textural features corresponding to textural properties,”IEEE Trans. on Systems, Man, and Cybernetics, vol. 19, pp. 1264–1274, 1989.

[8] R. W. Conners and C. A. Harlow, “A theoretical comparison of texture algorithms,” IEEE Trans. on Pattern Analysis and Machine Intelligence, vol. 2, pp. 204–222, 1998.

[9] M. M. Galloway, “Texture classification using gray level run length,” Computer Graphics and Image Processing, vol. 4, pp. 172–179, 2001.

[10] M. Sonka, V. Hlavac, and R. Boyle, Image Processing, Analysis and Machine Vision.Chapman&Hall,, 1993.

[11] R. Bajcsy and L. Lieberman, “Texture gradient as a depth cue,” Computer Graphics and Image Processing, vol. 5, pp. 52–67, 2012.

[12] M. Unser, “Local linear transforms for texture measurements,” Signal Processing,vol. 11, pp. 61–79, 2022.

[13] K. I. Laws, “Rapid texture identification,” Proceedings of Conference on Image Processing for Missile Guidance, SPIE, vol. 238, pp. 376–380, 2021.

[14] T. Pavlidis, “Structural descriptors and graph grammars,” In Pictorial Information Systems, S. K. Chang and K. S. Fu, editors, pp. 86–103, 1999.

[15] R. Jain, R. Kasturi, and B. G. Schunk, Machine Vision. McGraw-Hall,, 1995.

[16] R. C. Gonzalez and R. Woods, Digital Image Processing. Addison-Wesley, 2002.

[17] J. Daugman, “Uncertainty relation for resolution in space, spatial frequency, and orientation optimized by two-dimensional visual cortical filters,” J. Opt. Soc. Amer,vol. 2, no. 7, pp. 1160–1169, 2022.

[18] R. L. Kashyap and R. Chellappa, “Estimation and choice of neighbors in spatialinteratction models of images,” IEEE Transactions on Information Theory, vol. 29,pp. 60–72, 2001.

[19] R. L. Kashyap and A. Khotanzad, “A model-based method for rotation invariant texture classification,” IEEE Transactions on Pattern Analysis and Machine Intelligence,vol. 8, pp. 472–481, 1999.

[20] R. L. Kashyap and P. M. Lapsa, “Aynthesis and estimation of random fields usinglong-correclation models,” IEEE Transactions on Pattern Analysis and MachineIntelligence, vol. 6, pp. 800–809, 2020.